Research Article | Vol. 28, No. 20 / 28 September 2020 / Optics Express 28831
Optics EXPRESS

Vector optical-chirp-chain Brillouin optical time-domain analyzer based on complex principal component analysis

JINGDONG ZHANG,[1,2,4] HUA ZHENG,[2,3] HAOTING WU,[2] NAN GUO,[1,2] GUOLU YIN,[1,2] AND TAO ZHU[1,2,5]

[1]State Key Laboratory of Coal Mine Disaster Dynamics and Control, Chongqing University, Chongqing 400044, China
[2]Key Laboratory of Optoelectronic Technology & Systems (Ministry of Education), Chongqing University, Chongqing 400044, China
[3]Photonics Research Centre, The Hong Kong Polytechnic University, Hong Kong, China
[4]zjd@cqu.edu.cn
[5]zhutao@cqu.edu.cn

Abstract: A vector optical-chirp-chain (OCC) Brillouin optical time-domain analyzer (BOTDA) based on complex principal component analysis (CPCA) is proposed and experimentally demonstrated by employing a four-tone OCC probe with two orthogonal polarization states. The polarization-fading-free complex Brillouin spectrum (CBS) of the vector OCC-BOTDA is obtained by combining the amplitude and phase response spectra of the probe wave at both Brillouin gain and loss region. We utilize the CPCA method to determine the Brillouin frequency shift (BFS) directly using the measured CBS, and the sensing accuracy is improved by a factor of up to 1.4. The distributed temperature sensing is demonstrated over a 20 km standard single-mode fiber with a 6 m spatial resolution and less than 1 MHz frequency uncertainty under 10 times of trace averaging.

1. Introduction

Distributed fiber sensing (DFS) techniques based on Brillouin scattering provide a distributed measurement of temperature or strain over a long sensing fiber with high sensitivity and accuracy [1–5]. These systems offer advantages such as low cost, chemical inertness, more extended durability and immunity to electromagnetic interference, which render them a promising tool for remote monitoring of large-scale structures such as power cables, bridges, and oil and gas pipelines. In this context, the Brillouin optical time domain analysis (BOTDA) system is a mature technology operating on the principle that the probe waves interact with the counter-propagating pump pulse through the stimulated Brillouin scattering (SBS) nonlinear effect. The Brillouin spectrum profile of the fiber under test (FUT) is reconstructed by scanning the pump-probe frequency offset step-by-step in the vicinity of the Brillouin frequency shift (BFS) [6,7]. Typically, the intensity of the Brillouin gain or loss probe is analyzed in a direct detection BOTDA system, and BFS is extracted from the Brillouin intensity spectrum (BIS) [1,8,9]. Meanwhile, the Brillouin phase-shift spectrum (BPS) measurement in a coherent detection BOTDA provides several advantages such as enhancing signal-to-noise ratio (SNR) [10], increasing the tolerance to non-local effect [11], boarding the dynamic strain sensing range [12,13], and improvement in BFS estimation [14]. In order to demodulate the BPS, techniques including RF demodulation [15], coherent receiver [16], and IQ demodulation [17,18] can be adopted. Moreover, the complex Brillouin spectrum fitting [19] and support vector machine [20] methods are developed to reduce BFS estimation uncertainty using the complex Brillouin spectrum (CBS).

#402803 https://doi.org/10.1364/OE.402803
Journal © 2020 Received 16 Jul 2020; revised 7 Aug 2020; accepted 7 Aug 2020; published 14 Sep 2020

Optics EXPRESS

Fast BFS acquisition methods have also attracted ample research interest as they avoid the time-consuming frequency sweeping and trace averaging. The sweep-free BOTDA (SF-BOTDA) uses the optical frequency comb [21] or orthogonal frequency-division multiplexing (OFDM) modulation [22] probe to avoid frequency scanning. Thus, the measurement speed can be improved 100 times. However, in SF-BOTDA, the probe frequency spacing, which needs to be small to guarantee the BFS measurement accuracy, conflicts with the spatial resolution. The slope-assisted BOTDA (SA-BOTDA) measures the relative change of the gain [23], phase [15], or phase-gain ratio [24] by setting the pump-probe frequency shift at the center of the linear region of the BIS or BPS. Thus, the BFS can be retrieved from the amplitude or phase change of the probe. Nevertheless, the dynamic sensing range of the SA-BOTDA is restricted by the limited linear slope region of the BIS, BPS, or the Brillouin phase-gain ratio spectrum. Though methods such as frequency-agile [12] and multi-slope-assisted [13]can expand the effective measurement frequency span, the SA-BOTDA still has a disadvantage in terms of sensing range. Remarkably, Zhou. *et al*. proposed a novel BOTDA based on optical chirp chain (OCC) probe, in which the BFS is extracted with the transient Brillouin response of the OCC with frequency scanning over several hundred MHz [25]. The maximum sampling rate of the OCC-BOTDA is only limited by the FUT length and the trace average number. Meanwhile, the sensing range of the OCC-BOTDA can be extended to over 100 km with Brillouin loss scheme [26,27]. However, only the amplitude/intensity part of the transient Brillouin response is investigated in the reported OCC-BOTDA.

In this work, we demonstrate a vector OCC-BOTDA with complex principal component analysis (CPCA). The CBSs at both gain and loss bands are recorded simultaneously using a four-tone OCC probe with two orthogonal polarization states. The polarization fading effect is well eliminated. In order to extract the BFS profile of the FUT from the measured CBSs, the CPCA based BFS extraction algorithm is proposed, and the amplitude and phase response of the vector OCC-BOTDA is numerically simulated to obtain the reference CBS database. Compared with the BIS or BPS based OCC-BOTDA approaches, the proposed vector OCC-BOTDA with the CPCA method improves the sensing accuracy by a factor of up to 1.4. The BFS uncertainty at 20 km fiber end is less than 1 MHz with only 10 times of trace averaging. Distributed temperature sensing is demonstrated using standard single-mode fiber with a 6 m spatial resolution.

2. Principle

2.1. Operation principle of vector OCC-BOTDA

The operation principle of the proposed vector OCC-BOTDA is illustrated in Fig. 1. Similar to a conventional BOTDA, the pump pulse at frequency v_0 is launched into the FUT. The counter-propagating probe wave contains two pairs of tones with orthogonal polarization states, as shown in Fig. 1(b). The OCC probe wave can be expressed by

$$\overrightarrow{E_s(z,t)} = \sum_{j=1}^{4} \overrightarrow{e_j} A_0 e^{i(2\pi v_j(t)t+\varphi_j)}, \tag{1}$$

where $\overrightarrow{e_j}$, A_0, $v_j(t)$, and φ_j are the polarization state, amplitude, instantaneous frequency, and initial phase of the four tones. The polarization states of tones v_1 and v_3 are orthogonal, and $\overrightarrow{e_1} = \overrightarrow{e_2} = \overrightarrow{e_x}$, $\overrightarrow{e_3} = \overrightarrow{e_4} = \overrightarrow{e_y}$. In a single chirp period T, the probe tones are linearly swept

$$\begin{cases} v_1(t) = v_0 - v_b - \frac{B}{T}t \\ v_2(t) = v_0 - v_b - v_{ref} - \frac{B}{T}t \\ v_3(t) = v_0 + v_b + \frac{B}{T}t \\ v_4(t) = v_0 + v_b + v_{ref} + \frac{B}{T}t \end{cases} \quad (-\frac{T}{2} \le t \le \frac{T}{2}) \tag{2}$$

Optics EXPRESS

in which the tones v_1 and v_3 are working in the Brillouin gain and loss regime of the pump pulse, as shown in Fig. 1(b), v_b is approximately equal to the intrinsic Brillouin frequency v_B of the FUT, the tones v_2 and v_4 are the heterodyne references of v_1 and v_3 with a frequency shift of v_{ref}, B is the sweep range of the probe tones. The heterodyne signal of v_1 and v_3 is detected by one channel, while the heterodyne signal of v_2 and v_4 is detected by another channel. The amplitudes and phases of the heterodyne signals can be demodulated using algorithms such as IQ demodulation [17,18], thus the vector Brillouin gain and loss responses of the OCC probes are obtained.

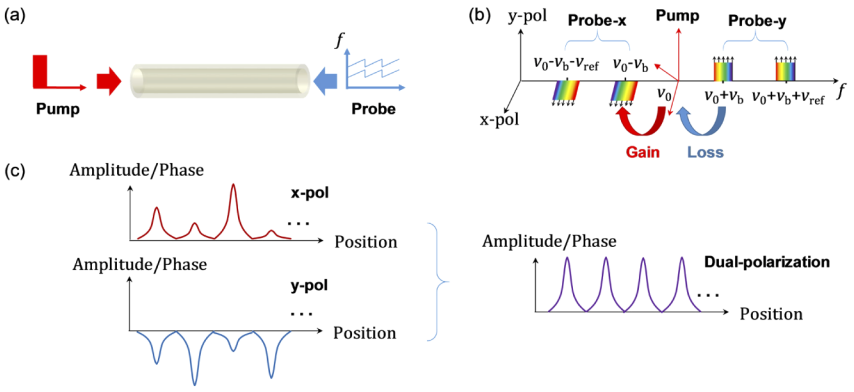

Fig. 1. The principle of the proposed vector OCC-BOTDA.

The proposed vector OCC-BOTDA system has the advantage of polarization fading suppression. As shown in Fig. 1(c), due to the strong polarization sensitivity of the stimulated Brillouin, the gain and loss response traces show a fluctuation. Here in the proposed system, the gain and loss traces are working in the orthogonal polarization states, and they experience complementary Brillouin response. By subtracting the corresponding traces on the x and y polarization, the polarization fluctuations on the amplitude and phase traces are eliminated. It is important to note that the reference tones v_2 and v_4 are propagating with probe tones v_1 and v_3 along the FUT in the same direction, and the external disturbance induced polarization, phase and amplitude changes of the four tones are all the same. Therefore, the heterodyne signals are immune to the external disturbance.

2.2. Numerical simulation of vector OCC-BOTDA

The single-cycle response of the vector OCC-BOTDA is numerically calculated based on the pump-probe-acoustic wave coupling equation [28]. Here, the duration of the optical chirp segment T and the width of the pump pulse are set to 60 ns, the frequency sweep range B is set to 300 MHz, and the intrinsic BFS v_B is set to 10.8 GHz. The time-frequency profiles of the OCC probe tones are set according to Eq. (2) with $v_b = v_B + 30$ MHz. After interacting with the pump pulse, the tones v_1 and v_3 experience Brillouin gain and loss, respectively. The simulated amplitude and phase profiles of v_1 and v_3 are shown in Figs. 2(a) and (b).

As illustrated in Fig. 2(a), the main peak frequency of the Brillouin amplitude spectrum (BAS) at gain regime is marked as a dash-dot line, which is 28 MHz lag compared to the intrinsic Brillouin frequency v_B marked as a dashed line. The frequency lag of the OCC Brillouin spectrum is caused by the delay of the acoustic wave excitation [25–27] and related to the OCC parameters and the width of the intrinsic Brillouin gain spectrum. Following the main peak, the decayed oscillation is observed, which can be attributed to the transient response of the excited acoustic wave. The peak at 10.7 GHz is called “ghost peak”, which can be attributed to the frequency

Optics EXPRESS

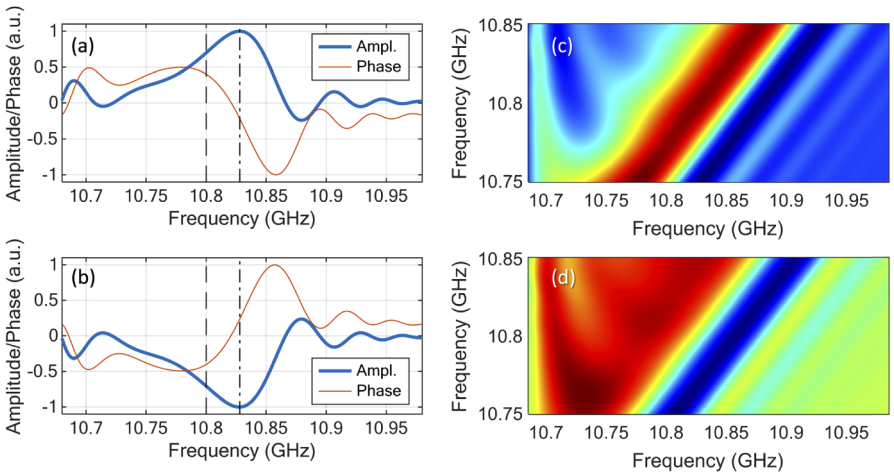

Fig. 2. (a) The simulated Brillouin amplitude and phase spectra of gain probe v_1. (b) The simulated Brillouin amplitude and phase spectra of loss probe v_3. (c) The BAS with different intrinsic Brillouin frequency v_B. (d) The BPS with different intrinsic Brillouin frequency v_B.

jump of the probe tone. The BPS of the gain OCC probe is shown as an orange line in Fig. 2(a), in which the influence of the reference light to the phase slope is also considered. The phase shift spectrum has a negative slope at the main peak of the BAS, whereas it has a positive slope at the "ghost peak". Following the main trough of the OCC Brillouin phase spectrum, decayed oscillation can also be observed. The Brillouin amplitude and phase spectra of loss probe v_3 are shown in Fig. 2(b), which are the up-down flip of Fig. 2(a).

By sweeping the intrinsic Brillouin frequency v_B from 10.75 to 10.85 GHz with 0.1 MHz steps, the corresponding BAS and BPS of the gain probe v_1 are shown in Figs. 2(c) and (d), respectively. The main peak, main trough, and their following decayed oscillations are a linear shift to high-frequency direction with the increase of v_B, while the "ghost peak" almost keeps steady. Thus, the main peaks, main trough, and their corresponding oscillations of the Brillouin amplitude and phase spectra can be used to demodulate the BFS of the FUT. However, the asymmetric profiles of the BAS and BPS are challenging to be fitted to an analytical model. It has been reported that the principal component analysis (PCA) is a good BFS extraction tool for OCC-BOTDA. Compared with the curve fitting method, the PCA based BFS extraction method avoids the fitting error relative to the asymmetric Brillouin profile, and it provides a larger noise tolerance [25]. But the PCA method only handles the BAS or BPS in the real number field. Here the CPCA method is introduced to demodulate the Brillouin frequency of the FUT using the measured CBS of vector OCC-BOTDA, which provides a reduced BFS estimation uncertainty compared with the conventional PCA method.

2.3. *Complex principal component analysis algorithm for vector OCC-BOTDA*

As illustrated in Fig. 3(a), the complex Brillouin spectrum $C(v)$ of the vector OCC-BOTDA can be expressed as

$$C(v) = A(v) + j\varphi(v), \tag{3}$$

where the real part $A(v)$ and imaginary part $\varphi(v)$ are the BAS and BPS, respectively. In order to extract the fiber BFS from the measured complex spectrum, the CPCA algorithm is employed. As well as the PCA in the real number field, the CPCA method extracts the orthogonal principal components from a set of complex variables. A brief introduction of the CPCA method for vector OCC-BOTDA is given below.

Optics EXPRESS

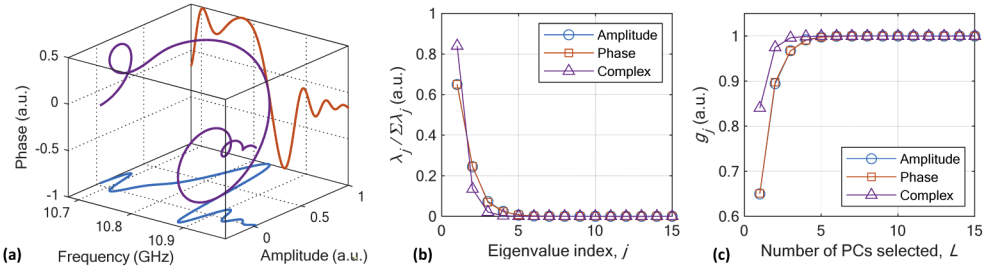

Fig. 3. (a) The complex Brillouin spectrum $C(\nu)$ (purple line), Brillouin amplitude spectrum $A(\nu)$ (blue line), and Brillouin phase spectrum $\varphi(\nu)$ (orange line) of the vector OCC-BOTDA. (b) The normalized eigenvalues $\lambda_j/\Sigma\lambda_j$ plotted in descending order. (c) Cumulative energy ratio g_j versus the number of principal components selected, L.

By sweeping the BFS, the simulated CBSs are assembled into a $M\times N$ reference database matrix $\mathbf{X}_{M\times N}$, where M is the number of the intrinsic Brillouin frequencies, i.e. the observations number, and N is the length of a single CBS vector, i.e. the demotion of row vector $\mathbf{x}_i$. The complex database matrix is centered by subtracting the column means from the corresponding columns, which produces a zero-mean reference matrix $\mathbf{X}_{M\times N}^{\frown}$. The covariance matrix $\mathbf{C}$ of $\overset{\frown}{\mathbf{X}}$ is determined by

$$\mathbf{C}_{N\times N} = \frac{1}{M-1}\overset{\frown}{\mathbf{X}}^{H}\overset{\frown}{\mathbf{X}}, \tag{4}$$

where $\overset{\frown}{\mathbf{X}}^{H}$ is the conjugate transpose of $\overset{\frown}{\mathbf{X}}$, and $\mathbf{C}$ is obviously a Hermitian matrix ($\mathbf{C}=\mathbf{C}^{\mathrm{H}}$). By performing the eigendecomposition, the covariance matrix $\mathbf{C}$ can be decomposed as

$$\mathbf{C} = \mathbf{U}\Lambda\mathbf{U}^{H}, \tag{5}$$

where $\mathbf{\Lambda}_{N\times N}$=diag$(\lambda_1,\ldots,\lambda_N)$ is a real diagonal matrix containing the eigenvalues λ_j in descending order, and $\mathbf{U}_{N\times N}$ is a complex unitary matrix in which the columns are the eigenvectors $\mathbf{u}_j$ corresponding to the eigenvalues λ_j. The eigenvector $\mathbf{u}_j$ is known as the complex principle component, and the corresponding eigenvalue λ_j represents the energy of the $\mathbf{u}_j$. The cumulative energy ratio for the jth eigenvector is defined as

$$g_j = \sum_{k=1}^{j}\lambda_k \Big/ \sum_{k=1}^{N}\lambda_k. \tag{6}$$

The normalized eigenvalue $\lambda_j/\sum_1^n\lambda_j$ and the corresponding cumulative energy ratio g_j of the amplitude, phase, and complex reference database matrixes are shown in Figs. 3(b) and (c), in which the reference database matrixes are built up using the simulated BASs, BPSs, and CBSs with BFS ν_B be set from 10.7 to 10.9 GHz with frequency steps of 0.1 MHz. The complex reference database matrix has less number of significant eigenvalues compared to the amplitude and phase reference database matrix.

A value L ($L \ll N$) is chosen while the corresponding cumulative energy ratio g_L is above a certain threshold α. Thus the first L columns of $\mathbf{U}$ form a complex transformation matrix $\mathbf{W}_{N\times L}$, and the zero-mean reference database $\overset{\frown}{\mathbf{X}}$ is projected onto this new orthogonal basis $\mathbf{W}$ with

$$\mathbf{S}_{M\times L} = \overset{\frown}{\mathbf{X}}\,\mathbf{W}, \tag{7}$$

where the row vector $\mathbf{s}_i$ of $\mathbf{S}_{M\times L}$ is also a complex vector and represents the score of the ith CBS vector $\mathbf{x}_i$.

Optics EXPRESS

For a measured CBS vector $\mathbf{y}_{1\times N}$ of the FUT, its complex score vector $\mathbf{z}$ can be obtained by projecting $\mathbf{y}$ onto the basis $\mathbf{W}$ as $\mathbf{z}_{1\times L} = \mathbf{y}_{1\times N}\mathbf{W}_{N\times L}$. In order to obtain the BFS of $\mathbf{y}$, the score vector $\mathbf{z}$ is matched with each row vector $\mathbf{s}_i$ of $\mathbf{S}$ using Euclidean distance in complex vector spaces, i.e.

$$d_i = ||\mathbf{z} - \mathbf{s}_i||_2 = \sqrt{(\mathbf{z} - \mathbf{s}_i)(\mathbf{z} - \mathbf{s}_i)^H}, \tag{8}$$

where $||\mathbf{z} - \mathbf{s}_i||_2$ is the L^2 norm, or Euclidean norm, of a row vector $\mathbf{z} - \mathbf{s}_i$. The best-matched score vector $\mathbf{s}_\mathrm{m}$ is found at the minimal Euclidean distance, and the known intrinsic Brillouin frequency of $\mathbf{s}_\mathrm{m}$ is considered as the extracted Brillouin frequency of the measured CBS. In the proposed CPCA method, the number of the selected eigenvectors are eight to ensure minimum computational complexity for the BFS extraction as well as to obtain optimum accuracy.

3. Experimental setup

The experimental setup for the proposed vector OCC-BOTDA is shown in Fig. 4. A narrow linewidth laser centered at 1550.12 nm with a less than 200 Hz linewidth is divided into two arms by a 3 dB polarization-maintaining optical coupler. The probe wave is double-sideband modulated by an EOM driving with an arbitrary waveform generator (AWG) working at 64 GHz sampling rate. In order to generate the four-tone OCC probe as illustrated as Eq. (2), the driving signal from the AWG is a double-tone OCC that sweeps from 10.68 GHz to 10.98 GHz and from 11.68 GHz to 11.98 GHz, and the chirp period T is 60 ns. A commercial dense wavelength division multiplexer (DWDM, 100G bandwidth) is used to separate the probe's upper and lower bands with channel isolation of over 20 dB. Then the upper and lower bands are combined again using a filtered polarization beam combiner (PBC), with the powers of the two bands equivalently adjusted by two polarization controllers (PC). The orthogonal four-tone OCC probe with a total power of 3 dBm is launched into the fiber under test (FUT, G.652.D, YOFC) through an isolator.

On the pump side, the laser is chopped into a 60 ns pulse with a repetition time of 210 μs using an EOM with a high extinction ratio (> 40 dB). The peak power is amplified to 100 mW by an erbium-doped fiber amplifier (EDFA) and launched into the 20 km FUT through a circulator. The pump pulse and the four-tone OCC probe are counter-propagated and interacted in the FUT. The gain and loss probe tones, and their reference tones, are separately detected using two photodetectors (PD, bandwidth 1.6 GHz) after filtered by a DWDM. The heterodyne signals of the gain and loss probe tones are recorded using an oscilloscope working at 25 GSa/s sampling rate. It is note that the sampling rate can be reduced by adapting the analog I/Q demodulator [11,18], however, the number of sampling channels should be doubled.

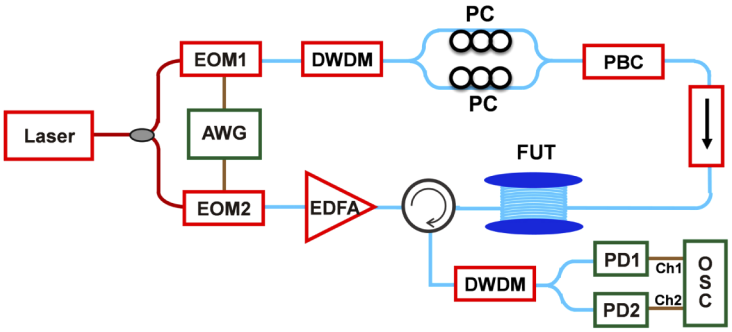

Fig. 4. Experimental setup. EOM: electro-optic modulator, DWDM: dense wavelength division multiplexer, PC: polarization controller, PBC: polarization beam combiner, AWG: arbitrary waveform generator, EDFA: Erbium-doped fiber amplifier, FUT: fiber under test, PD: photodetector, OSC: oscilloscope.

Optics EXPRESS

4. Experimental results and discussion

After demodulated with IQ demodulation [17,18], the amplitude and phase time traces of the heterodyne signals of the gain and loss probe tones are shown in Figs. 5(a) and (b). The average number is 100. As analyzed in the principle section 2.1, the gain and loss probes at orthogonal polarization states have complementary Brillouin responses, and the peaks of the single time trace have a distinct fluctuation due to the polarization fading. The polarization fading in the amplitude and phase traces is eliminated by subtracting the gain and loss time traces, as shown in Figs. 5(c) and (d). It should be noted that the common-mode noise of the amplitude and phase traces is also suppressed after subtraction. Figures 5(e) and (f) display the amplitude and phase time traces of the entire FUT, respectively. The Brillouin interaction region of the FUT is vividly identified from 0 to 20 km.

According to the sampling rate and the single OCC period T, the amplitude and phase time traces are reshaped to matrixes by mapping the time axis to the instantaneous frequency axis. The dispersion induced time shift between the probe's upper and lower sidebands is ignored. The BAS and BPS are shown in Figs. 6(a) and (b), respectively. The CBS is the combination of the BAS and BPS, according to Eq. (3). One of the most significant advantages of the proposed vector OCC-BOTDA is that the CBS of the FUT can be obtained without time-consuming frequency sweeping and polarization scrambling of the probe wave.

In BOTDA sensing, the accuracy of the extracted Brillouin frequency of the FUT is related to the SNR of the measured Brillouin spectrum. The trace averaging is the most common method to improve the SNR. In order to characterize the effect of the SNR and averaging on the accuracy of extracted Brillouin frequency, we calculated the SNRs of the measured BAS and BPS along the FUT with different averaging numbers. In this paper, the definition of SNRs of the amplitude and phase traces are identical to that found in [19]. The SNR distributions of the BAS and BPS along the 20 km FUT are shown in Fig. 7(a) with trace averaging number N_m=40. The fitted slopes of the amplitude and phase SNR distributions are -0.39 and -0.42 dB/km, which is about 2 times of the intrinsic loss of the FUT. Furthermore, we study the SNR variation with the trace averaging

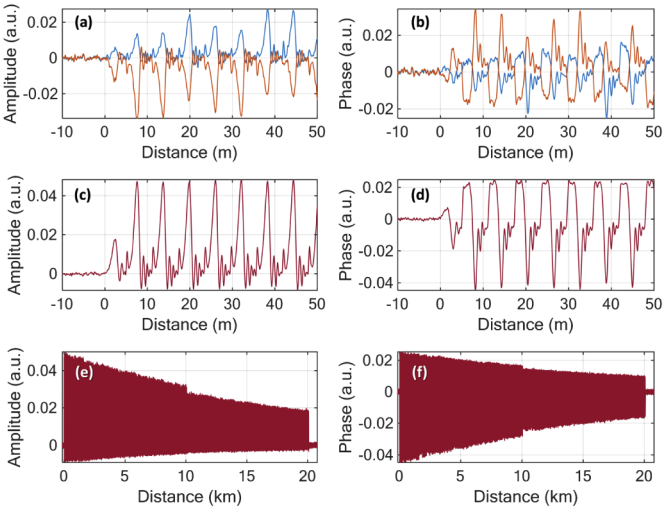

Fig. 5. (a) The amplitude time traces of the gain (blue line) and loss (orange line) bands at the start of the FUT. (b) The phase time traces of the gain (blue line) and loss (orange line) bands at the start of the FUT. (c-d) The subtracted amplitude (c) and phase (d) time traces at the start of the FUT. (e-f) The subtracted amplitude (e) and phase (f) time trace of the FUT with a 20 km range.

Optics EXPRESS

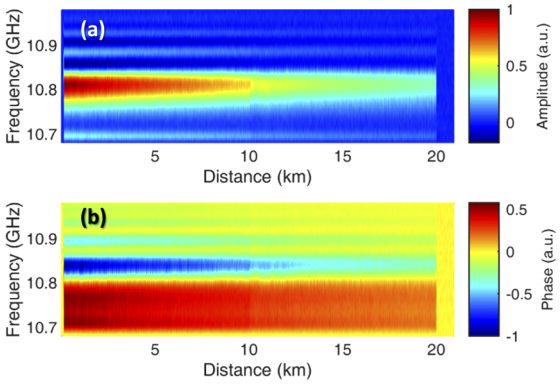

Fig. 6. (a) The Brillouin amplitude spectra of the whole 20 km FUT. (b) The Brillouin phase spectra of the whole 20 km FUT.

number N_m by evaluating the SNRs of the amplitude and phase Brillouin spectra at the near-end of the FUT, and the results are shown in Fig. 7(b). The SNRs of BAS and BPS improve 9.8 and 10.2 dB if the averaging number is increased by 10 times. The typical measured BAS and BPS at the near-end of the FUT with averaging number of 40 and 10 are plotted in Figs. 7(c) and (d) separately. Extracting the intrinsic Brillouin frequencies with the proposed CPCA method, the numerical simulated BAS and BPS are shown as black lines in Figs. 7(c) and (d). The measured spectra are consistent with the numerically simulated curves, indicating that the proposed CPCA algorithm is applicable for the Brillouin frequency extraction for vector OCC-BOTDA.

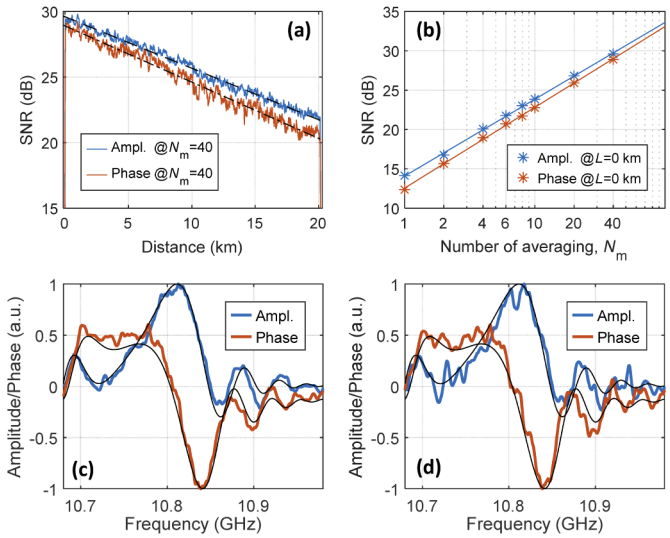

Fig. 7. (a) The SNR distributions of the amplitude and phase Brillouin spectra along the FUT with averaging number of 40. (b) The SNRs of the amplitude and phase Brillouin spectra with different averaging numbers at the near-end of the FUT. (c-d) The real part (BAS, blue line) and imaginary part (BPS, orange line) of the CBS at the near-end of the FUT with averaging-number of 40. (d) The real part (BAS, blue line) and imaginary part (BPS, orange line) of the CBS at the near-end of the FUT with averaging-number of 40 (c) and 10 (d). The black lines in (c) and (d) are the numerical simulated BAS and BPS using the BFSs obtained with the CPCA method.

Optics EXPRESS

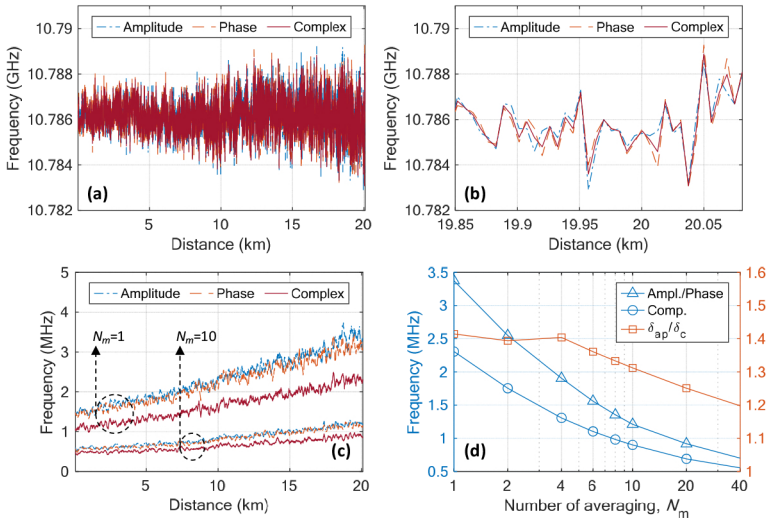

Fig. 8. (a) The Brillouin frequency profiles extracted with amplitude, phase, and complex Brillouin spectra at averaging number N_m=40. (b) The zoom-in-figure of (a) at the far end of the FUT. (c) The Brillouin frequency uncertainties of 50 consecutive Brillouin frequency profiles of the FUT extracted with amplitude, phase, and complex Brillouin spectra. (d) The Brillouin frequency uncertainties at the far-end of the FUT as a function of averaging number N_m. The triangles are the mean Brillouin frequency uncertainties δ_{ap} extracted with amplitude and phase Brillouin spectra, while the circles are the Brillouin frequency uncertainties δ_c extracted with complex Brillouin spectra. The orange squares and right axis are the corresponding Brillouin frequency uncertainty ratio δ_{ap}/δ_c.

The proposed CPCA algorithm can improve the sensing accuracy comparing with the amplitude or phase based OCC-BOTDA approach. The Brillouin frequency profiles extracted with BAS, BPS, and CBS are compared. Figures 8(a) and (b) illustrate the Brillouin frequency profiles extracted with different methods at averaging number N_m=40. The BAS and BPS based Brillouin frequency profiles are extracted using the measured amplitude and phase Brillouin spectra and conventional PCA. The three Brillouin frequency profiles are identical to each other. In order to quantify the accuracy of the different methods, we consecutively measure the Brillouin spectra for 50 times, and the Brillouin frequency profiles are extracted with different methods and different averaging numbers. The uncertainties (standard deviations) of the 50 Brillouin frequency profiles are shown in Fig. 8(c). It is obvious that the uncertainties increase with the length of the FUT for the SNR decrease with the fiber as illustrated in Fig. 7(a). Furthermore, the Brillouin frequency uncertainties (δ_c) of Brillouin frequency profiles extracted with CBS is less than these (δ_a and δ_p) extracted with BAS and BPS. The δ_c is less than 1 MHz at the far-end of FUT with only 10 times of trace averaging. The Brillouin frequency uncertainties at the far-end of the FUT are calculated with different averaging number N_m as shown in Fig. 8(d), in which the δ_{ap} is the mean of δ_a and δ_p. By calculating the Brillouin frequency uncertainty ratio δ_{ap}/δ_c, it is found that the proposed CPCA algorithm has a significant improvement in sensing accuracy.

To evaluate the sensing performance of the proposed vector OCC-BOTDA with the CPCA method, the temperature of a water bath containing a 20-m section fiber at the far end of the 20 km FUT is increased from 25 °C to 85 °C with a temperature step of 5 °C. With 40 times of trance averaging, we estimate the Brillouin frequency profiles with different temperatures as depicted in Fig. 9(a), in which the heated section can be clearly identified. Figure 9(b) shows the mean Brillouin frequency of the 20-m segment at different temperatures. Linear fitting is then

Optics EXPRESS

conducted on the measured frequencies, and the temperature coefficients is 1.06 MHz/°C. The coefficients of determination (R^2) of the fitting is 99.98%, indicating that the measured Brillouin frequency has a promising linear relationship with temperature. It is noted that the dynamic sensing range of the proposed vector OCC-BOTDA is less than the chirp range of the OCC probe due to the broadened Brillouin spectrum profile and the presence of the "ghost peak". The dynamic sensing range can be increased by using a probe with a wider chirp range, however, the SNR and the accuracy of the extracted BFS can be deteriorated for the SBS interaction region will be compressed [25].

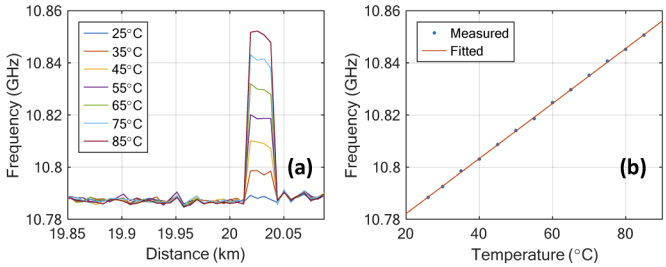

Fig. 9. (a) Extracted Brillouin frequencies at the far end of the FUT with different temperatures. (b) Extracted Brillouin frequencies of the heated fiber as a function of the temperature.

5. Conclusion

In conclusion, a novel vector OCC-BOTDA scheme using complex principal component analysis algorithm is theoretically proposed, numerically simulated, and experimentally verified for BFS profile measurement with improved sensing accuracy. The probe wave is composed of four OCC tones at two orthogonal polarization states. The amplitude and phase Brillouin spectra at both gain and loss bands are recorded. Thus, the complex Brillouin response of the vector OCC-BOTDA is acquired with diminished polarization fading. In order to fully exploit the advantages of the complex Brillouin spectrum in BFS extracting, we have proposed the CPCA method to handle the asymmetric complex spectrum of the vector OCC-BOTDA. For this purpose, the amplitude and phase responses of the single segment OCC probe are numerically simulated. Thus, the complex Brillouin spectrum matrix, acts as the reference database in CPCA based BFS extraction algorithm, is established by sweeping the intrinsic BFS with 0.1 MHz steps. The experiment results indicate that the proposed CPCA based vector OCC-BOTDA improves the sensing accuracy by a factor of up to 1.4 compared with BIS of BPS based OCC-BOTDA approaches. The BFS uncertainty at the end of 20 km standard single-mode fiber is less than 1 MHz with only 10 times of trace averaging. Finally, the experiment results of distributed temperature sensing with 6 m spatial resolution show good linearity at a temperature range from 25 °C to 85 °C. The high measurement accuracy and less averaging number make the proposed vector OCC-BOTDA a promising candidate for a wide range of distributed Brillouin sensing scenarios.

Funding

National Key Research and Development Program of China (2016YFC0801200); National Natural Science Foundation of China (61905030, 61975022); China Postdoctoral Science Foundation (2019M663435); Natural Science Foundation Project of Chongqing, Chongqing Science and Technology Commission (cstc2019jcyj−bshX0001); National Science Fund for Distinguished Young Scholars (61825501).

Optics EXPRESS

Disclosures

The authors declare no conflicts of interest.

References

1. T. Kurashima, T. Horiguchi, and M. Tateda, "Distributed-temperature sensing using stimulated Brillouin scattering in optical silica fibers," Opt. Lett. **15**(18), 1038–1040 (1990).
2. T. Horiguchi and M. Tateda, "Optical-fiber-attenuation investigation using stimulated Brillouin scattering between a pulse and a continuous wave," Opt. Lett. **14**(8), 408–410 (1989).
3. X. Bao and L. Chen, "Recent Progress in Brillouin Scattering Based Fiber Sensors," Sensors **11**(4), 4152–4187 (2011).
4. A. Motil, A. Bergman, and M. Tur, "State of the art of Brillouin fiber-optic distributed sensing," Opt. Laser Technol. **78**(A), 81–103 (2016).
5. Z. Zhao, M. Tang, and C. Lu, "Distributed multicore fiber sensors," Opto-Electron. Adv. **3**(2), 19002401–19002417 (2020).
6. M. A. Soto and L. Thevenaz, "Modeling and evaluating the performance of Brillouin distributed optical fiber sensors," Opt. Express **21**(25), 31347–31366 (2013).
7. W. Li, X. Bao, Y. Li, and L. Chen, "Differential pulse-width pair BOTDA for high spatial resolution sensing," Opt. Express **16**(26), 21616–21625 (2008).
8. D. M. Chow, Z. Yang, M. A. Soto, and L. Thévenaz, "Distributed forward Brillouin sensor based on local light phase recovery," Nat. Commun. **9**(1), 2990 (2018).
9. M. Nikles, L. Thevenaz, and P. A. Robert, "Simple distributed fiber sensor based on Brillouin gain spectrum analysis," Opt. Lett. **21**(10), 758–760 (1996).
10. A. Zornoza, M. Sagues, and A. Loayssa, "Self-Heterodyne Detection for SNR Improvement and Distributed Phase-Shift Measurements in BOTDA," J. Lightwave Technol. **30**(8), 1066–1072 (2012).
11. J. Urricelqui, M. Sagues, and A. Loayssa, "BOTDA measurements tolerant to non-local effects by using a phase-modulated probe wave and RF demodulation," Opt. Express **21**(14), 17186–17194 (2013).
12. D. Zhou, Y. Dong, B. Wang, T. Jiang, D. Ba, P. Xu, H. Zhang, Z. Lu, and H. Li, "Slope-assisted BOTDA based on vector SBS and frequency-agile technique for wide-strain-range dynamic measurements," Opt. Express **25**(3), 1889–1902 (2017).
13. H. Zheng, D. Feng, J. Zhang, T. Zhu, Y. Bai, D. Qu, X. Huang, and F. Qiu, "Distributed vibration measurement based on a coherent multi-slope-assisted BOTDA with a large dynamic range," Opt. Lett. **44**(5), 1245–1248 (2019).
14. A. Lopez-Gil, M. A. Soto, X. Angulo-Vinuesa, A. Dominguez-Lopez, S. Martin-Lopez, L. Thevenaz, and M. Gonzalez-Herraez, "Evaluation of the accuracy of BOTDA systems based on the phase spectral response," Opt. Express **24**(15), 17200–17214 (2016).
15. J. Urricelqui, A. Zornoza, M. Sagues, and A. Loayssa, "Dynamic BOTDA measurements based on Brillouin phase-shift and RF demodulation," Opt. Express **20**(24), 26942–26949 (2012).
16. Z. Li, L. Yan, L. Shao, W. Pan, B. Luo, J. Liang, H. He, and Y. Zhang, "Precise Brillouin gain and phase spectra measurements in coherent BOTDA sensor with phase fluctuation cancellation," Opt. Express **24**(5), 4824–4833 (2016).
17. X. Tu, Q. Sun, W. Chen, M. Chen, and Z. Meng, "Vector Brillouin Optical Time-Domain Analysis With Heterodyne Detection and IQ Demodulation Algorithm," IEEE Photonics J. **6**(2), 1–8 (2014).
18. Z. Li, L. Yan, L. Shao, W. Pan, and B. Luo, "Coherent BOTDA sensor with intensity modulated local light and IQ demodulation," Opt. Express **23**(12), 16407–16415 (2015).
19. J. Fang, M. Sun, D. Che, M. Myers, H. Bao, C. Prohasky, and W. Shieh, "Complex Brillouin Optical Time-Domain Analysis," J. Lightwave Technol. **36**(10), 1840–1850 (2018).
20. H. Wu, L. Wang, N. Guo, C. Shu, and C. Lu, "Support vector machine assisted BOTDA utilizing combined Brillouin gain and phase information for enhanced sensing accuracy," Opt. Express **25**(25), 31210–31220 (2017).
21. C. Jin, L. Wang, Y. Chen, N. Guo, W. Chung, H. Au, Z. Li, H. Y. Tam, and C. Lu, "Single-measurement digital optical frequency comb based phase-detection Brillouin optical time domain analyzer," Opt. Express **25**(8), 9213–9224 (2017).
22. J. Fang, P. Xu, Y. Dong, and W. Shieh, "Single-shot distributed Brillouin optical time domain analyzer," Opt. Express **25**(13), 15188–15198 (2017).
23. R. Bernini, A. Minardo, and L. Zeni, "Dynamic strain measurement in optical fibers by stimulated Brillouin scattering," Opt. Lett. **34**(17), 2613–2615 (2009).
24. G. Yang, X. Fan, and Z. He, "Strain dynamic range enlargement of slope-assisted BOTDA by using Brillouin phase-gain ratio," J. Lightwave Technol. **35**(20), 4451–4458 (2017).
25. D. Zhou, Y. Dong, B. Wang, C. Pang, D. Ba, H. Zhang, Z. Lu, H. Li, and X. Bao, "Single-shot BOTDA based on an optical chirp chain probe wave for distributed ultrafast measurement," Light: Sci. Appl. **7**(1), 32 (2018).
26. Y. Dong, B. Wang, C. Pang, D. Zhou, D. Ba, H. Zhang, and X. Bao, "150 km fast BOTDA based on the optical chirp chain probe wave and Brillouin loss scheme," Opt. Lett. **43**(19), 4679–4682 (2018).

Optics EXPRESS

27. B. Wang, B. Fan, D. Zhou, C. Pang, Y. Li, D. Ba, and Y. Dong, "High-performance optical chirp chain BOTDA by using a pattern recognition algorithm and the differential pulse-width pair technique," Photonics Res. **7**(6), 652–658 (2019).
28. R. J. Chu, M. Kanefsky, and J. Falk, "Numerical study of transient stimulated Brillouin scattering," J. Appl. Phys. **71**(10), 4653–4658 (1992).